

Redox-Active Porous Organic Polymers for Energy Storage

Chang Wan Kang and Seung Uk Son*

*Department of Chemistry, Sungkyunkwan University, Suwon 16419, Korea. *E-mail: sson@skku.edu*

Received October 13, 2020, Accepted December 18, 2020, Published online December 29, 2020

This review introduces synthesis and energy storage applications of recent redox-active porous organic polymer (POP) materials. First, various redox-active molecular systems were summarized and then, synthetic examples of redox-active POP bearing the redox-active molecular moieties were described. Various synthetic strategies based on diverse coupling reactions of building blocks were described. In addition, postsynthetic modification strategies for the preparation of redox-active POP were described. Second, structures and electrochemical features of battery and pseudocapacitor devices were introduced. Then, electrochemical performance of various redox-active POP materials was summarized and described. Finally, merits and weak points of redox-active POPs as electrode materials were discussed and future research direction was suggested.

Keywords: Porous organic polymer, Battery, Pseudocapacitor, Redox, Energy storage

Introduction

As portable electronic devices have spread in human society, energy storage in rechargeable batteries and supercapacitors has become an important research subject.¹ During the last two decades, there have been numerous progresses in the development of new energy storage materials.² Reversible redox conversions of various materials have been utilized as chemical principles of electrical energy storage. Most related studies have focused inorganic electrode materials such as silicon, tin, carbon materials, metal oxides, and metal chalcogenides.³

Recently, organic electrode materials have attracted renewed attention of scientists.⁴ The merits of organic electrode materials can be summarized as follows. First, organic electrode materials can be chemically engineered from biomass.⁵ The renewable feature of biomass can induce sustainable chemistry of energy storage devices.⁵ Second, because organic electrode materials are free from heavy metals, they are more environmental-friendly than inorganic ones. Third, due to their unique flexible features, organic electrode materials are very promising in the engineering of flexible energy storage devices. Fourth, due to the relatively facile and diverse synthetic methodologies of organic materials, the electrochemical performance parameters such as cell potentials and capacities can be easily controlled through tailored chemical modification.

In this regard, redox-active molecular organic compounds have been studied as electrode materials of batteries.⁶ However, gradual dissolution of organic electrode materials into electrolytes can result in the gradual loss of storage capacities. In addition, intermediate cationic or anionic radical species generated by the single electron oxidation or reduction of neutral organic compounds are subject to dimerization, resulting in the loss of the original

redox performance. To overcome these problems, the networking of redox-active molecular compounds is a promising strategy to achieve advanced organic electrode materials.

Recently, (amorphous) porous organic polymer (POP) has been prepared through the networking of organic building blocks.⁷ Various coupling reactions of rigid organic building blocks induced the microporosity and high surface areas of POPs. Due to their cross-linked features, resultant POP materials are insoluble in common solvent including electrolyte solution. Due to the high surface area, porosity, and chemical stability, the functional sites of POP can be utilized in the various applications.⁷

Redox-active functionality can be incorporated into the POPs through two strategies.⁷ First, a predesigned building block approach⁸ can be applied to achieve the redox-active POPs. Usually, coupling functional groups are introduced into the redox-active molecules. And then, the resultant redox-active building blocks can be coupled through various organic reactions. Second, redox-active functionality can be incorporated into the POP through a postsynthetic modification strategy.⁹ In this case, after POP platforms are prepared by the coupling of relatively simple organic building blocks, the tailored redox-active moieties can be further introduced into the POP through side group or main chain postsynthetic modification.

In addition, to further enhance electrochemical performance of redox-active POP materials, their morphologies can be engineered by hard and soft template synthesis.¹⁰ For example, hollow redox-active POP materials with thin shell thicknesses could be prepared by the coupling of organic building blocks on the surface of nanoscaled silica templates. The etching of silica templates results in the formation of hollow POP materials.¹¹ Due to the empty inner space and thin shell thickness, electrolyte solution can be

easily diffused into hollow POP materials, resulting in the enhanced utilization of redox-active sites in the materials. In addition, nano-sized POP materials have been prepared by polymeric surfactants through the kinetic control of growth.¹²

Recently, there have been significant studies on the development of redox-active POPs for energy storage applications.^{13–25} While redox-active metal–organic framework (MOF) and covalent organic framework (COF) have been reviewed, the redox-active (amorphous) POP materials have been relatively less reviewed.⁴ In this review paper, we introduce the recent examples of redox-active POP materials for energy storage. Especially, this review focuses on redox-active molecular species and synthetic strategies for the redox-active POPs, which will be helpful in the designed synthesis of POP-based electrode materials for battery and pseudocapacitor applications.

Carbonyl-Based Redox Species and POP

One of the representative organic redox species is benzoquinone (Figure 1). Because the benzoquinone shows reversible two-electron redox reaction, benzoquinone-based POP can be a promising electrode material. Recently, Han *et al.* reported the preparation of benzoquinone-based POP, denoted by Poly-P5Q¹³ (Figure 1).

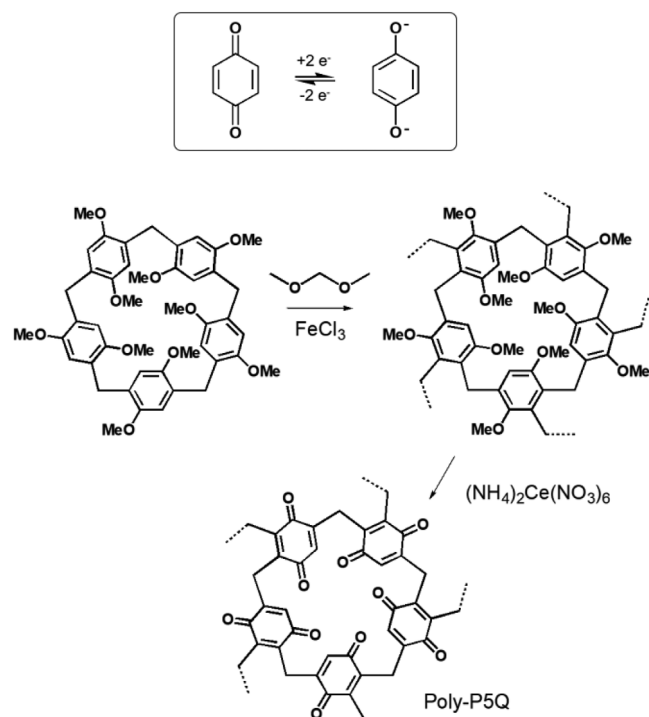


Figure 1. The redox reaction of benzoquinone and the synthesis of MOP-bearing benzoquinones through networking based on Friedel–Craft reaction. Reproduced under permission of ref. 13. Copyright 2017, Elsevier.

They used a macrocyclic compound, dimethoxypillar[5]arene (DMpillar[5]arene), as a starting compound. Through the FeCl₃-catalyzed Friedel–Craft reaction in the presence of dimethoxymethane, the hypercrosslinked polymer of DMpillar[5]arene was obtained. The Ce-mediated oxidation of dimethoxyarene rings resulted in the generation of benzoquinone moieties in the Poly-P5Q. The surface area of the Poly-P5Q was measured to be 104 m²/g. While the Poly-P5Q showed heterogeneous porous structure, mainly, mesoporosity was observed in the range of 2–5 nm. The Poly-P5Q was thermally stable up to 120°C.

Similar to benzoquinone, anthraquinone is a very useful redox compound showing reversible two-electron redox reaction (Figure 2). Additional side benzene rings of anthraquinone can be utilized in the introduction of various functional groups including coupling functional groups. Recently, Marcilla and coworkers reported the preparation of anthraquinone-based redox-active POP (IEP-11-E12).¹⁴ (Figure 2).

Basically, the IEP-11-E12 was prepared by the Sonogashira coupling of 1,3,5-triethynylbenzene with 2,6-dibromoanthraquinone. Especially, the POP materials were prepared through formation of mini-emulsions using a mixture of toluene, triethylamine, and water, resulting in a mixture of nanoparticles with diameters of 200–300 nm and nanowires with widths of 10–20 nm. Finally, the intermediate POP materials were further treated under solvothermal conditions to form IEP-11-E12.

Through the combination of mini-emulsion method and solvothermal treatment, highly porous IEP-11-E12 materials could be obtained. While conventional Sonogashira-based synthesis resulted in irregular POP (IEP-11-C) with a surface area of 609 m²/g, the IEP-11-E12 showed a high surface area up to 2200 m²/g. Interestingly, as solvothermal treatment time increased from 6 h to 12 h, the surface areas

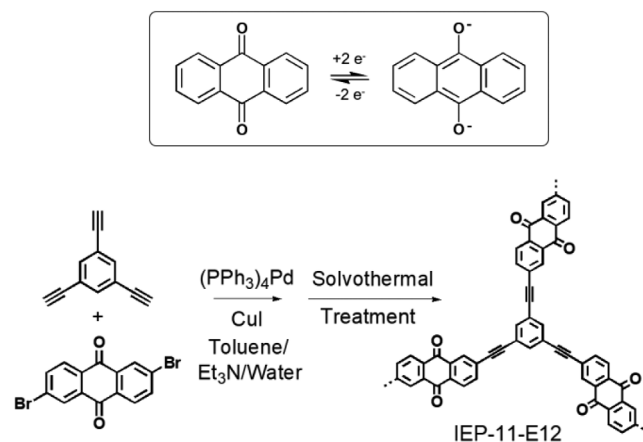


Figure 2. Two-electron redox reaction of anthraquinone and synthesis of anthraquinone-based POP materials by the Sonogashira coupling of 1,3,5-triethynylbenzene with 2,6-dibromoanthraquinone. Reproduced under permission of ref. 14. Copyright 2020, Wiley-VCH.

increased from 961 m²/g to 2200 m²/g. While the IEP-11-C showed conventional microporosity (pore sizes <2 nm), the IEP-11-E12 showed a dual porous feature with mesoporosity in the range of 2–15 nm and conventional microporosity. The IEP-11-E12 showed better dispersion ability in acetone than IEP-11-C, due to its nanostructural nature. In addition, in the engineering of thin film, more compact layers (three times thinner) could be engineered, compared with the cases of IEP-11-C.

Next redox-active organic systems are aromatic compounds with diacyl groups, which show two-electron redox conversions (Figure 3). In 2018, Son and co-workers reported the preparation of hollow POP materials bearing 1,4-di(3-phenylpropynoyl)benzene moieties (denoted by H-CMP-BPPB).¹⁵ (Figure 3).

The H-CMP-BPPB was prepared by the carbonylative Sonogashira coupling of 2 equiv 1,3,5-triethynylbenzene with 3 equiv 1,4-diiodobenzene in the presence of carbon monoxide. While the conventional Sonogashira coupling results in the coupling of terminal alkynes with aryl halides, the carbonylative Sonogashira coupling induces the insertion of carbonyl group between alkynes and arenes. Especially, in the synthesis of H-CMP-BPPB, POP materials were formed on the surface of silica spheres. The silica etching through treatment with HF solution resulted in the hollow H-CMP-BPPB materials with an average diameter of 218 nm and an average shell thickness of 23 nm.

The insertion of carbonyl groups in the H-CMP-BPPB was characterized by infrared (IR) absorption and solid state ¹³C nuclear magnetic resonance (NMR) spectroscopy. The strong vibration peak of carbonyl groups was observed at 1645 cm⁻¹. In ¹³C NMR spectrum, the carbonyl ¹³C peak appeared at 175 ppm, which was confirmed by the model compound. The content of incorporated carbonyl groups in H-CMP-BPPB was measured to ~6.69 mmol/g by elemental analysis. The surface areas of H-CMP-BPPB were measured to be 622 m²/g with typical microporosity

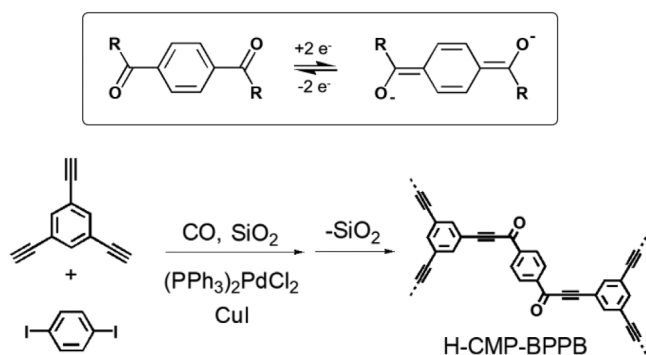


Figure 3. Two-electron redox conversion of 1,4-diacylbenzene and the synthesis of hollow POP materials bearing 1,4-di(3-phenylpropynoyl)benzenes through carbonylative Sonogashira coupling of 1,3,5-triethynylbenzene with 1,4-diiodobenzene in the presence of carbon monoxide. Reproduced under permission of ref. 15. Copyright 2018, Royal Society of Chemistry.

(a micropore volume of 0.18 cm³/g). The H-CMP-BPPB was thermally stable up to 303°C.

Further dicarbonyl and multicarbonyl compounds such as benzil and phenanthrene-9,10-dione are redox-active and have been studied in the synthesis of organic electrode materials.¹⁶ Especially, pyrene-4,5,9,10-tetraone is a very promising redox-active organic unit because it shows a four-electron redox reaction (Figure 4).

In 2020, Wang and coworkers reported the preparation of conjugated microporous polymer bearing pyrene-4,5,9,10-tetraone moieties (denoted by PT-BTA) through the Suzuki coupling of 2,7-dibromopyrene-4,5,9,10-tetraone and 1,3,5-tris(4,4,5,5-tetramethyl-1,2-dioxaborolan-2-yl)benzene.¹⁷ The PT-BTA showed a characteristic IR peak of carbonyl groups at 1682 cm⁻¹ and was thermally stable up to 200°C.

Noncarbonyl-Based Redox Species and POP

Recently, redox-active POP bearing noncarbonyl species also have been prepared by the coupling of pre-designed building blocks and by the postsynthetic introduction of redox-active species to POP. For example of noncarbonyl redox-active species, 1,1,4,4-tetracyanobutadiene derivatives with substituents show two-electron redox conversion, as shown in Figure 5.

In 2017, Son and coworkers reported that the postsynthetic modification strategy can be applied to introduce 1,1,4,4-tetracyanobutadiene species into POP.¹⁸ At first, POP bearing internal alkynes with electron-rich aryl groups was prepared by the Sonogashira coupling of tri(4-ethynylphenyl)amine with tri(4-iodophenyl)amine. For the template synthesis of hollow POP materials, ZIF-8 was

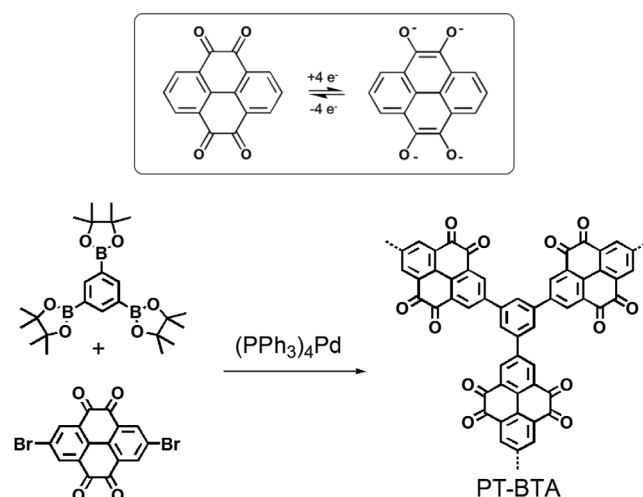


Figure 4. Four electron redox conversion of pyrene-4,5,9,10-tetraone and the synthesis of POP bearing pyrene-4,5,9,10-tetraone moieties by the Suzuki coupling of 2,7-dibromopyrene-4,5,9,10-tetraone and 1,3,5-tris(4,4,5,5-tetramethyl-1,2-dioxaborolan-2-yl)benzene. Reproduced under permission of ref. 17. Copyright 2020, Royal Society of Chemistry.

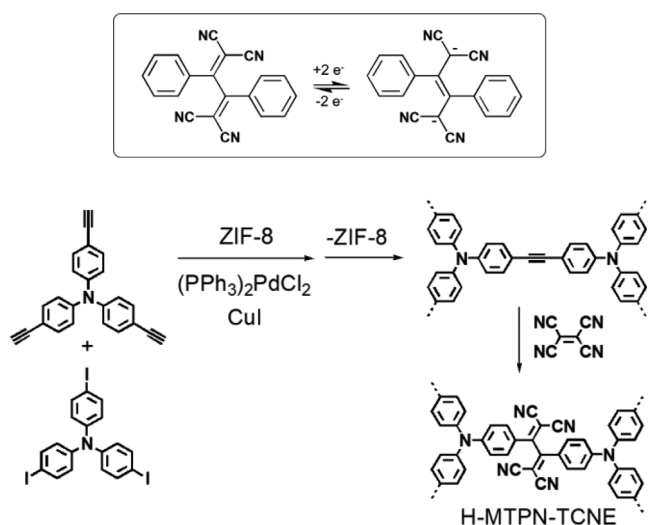


Figure 5. Two-electron redox conversion of 1,1,4,4-tetracyanobutadiene and the synthesis of redox-active POP through post-synthetic modification of POP through the reaction with tetracyanoethylene. Reproduced under permission of ref. 18. Copyright 2017, Royal Society of Chemistry.

used as a template. The successive reaction of hollow POP materials with a tetracyanoethylene reagent resulted in generation of 1,1,4,4-tetracyanobutadiene moieties in the POP. The resultant material was denoted by H-MTPN-TCNE.

The original orange color of POP changed to black (H-MTPN-TCNE with additional absorption band at 489 nm) through the postsynthetic modification, due to the photo-induced intramolecular charge transfer from the electron-rich triphenylamine moieties to the electron-deficient 1,1,4,4-tetracyanobutadiene moieties. Through the postsynthetic modification, the surface areas decreased from 767 m²/g to 589 m²/g. The vibration peak of cyano groups of H-MTPN-TCNE was observed at 2221 cm⁻¹. Through elemental analysis, the incorporated 1,1,4,4-tetracyanobutadiene species in the H-MTPN-TCNE was calculated as 1.3 mmol/g.

Viologens are dipyridinium salts and electron-deficient systems. The viologens are known to show their unique two-electron redox conversion (Figure 6).

In 2012, Son *et al.* reported the synthesis of POP-bearing viologens by the Sonogashira coupling of tetra(4-ethynylphenyl)methane with viologen salts bearing two di(4-iodophenyl) substituents.¹⁹ The resultant POP was denoted by MONT. Interestingly, due to unique self-templating reaction, the MONT showed tubular morphologies with a wall thickness of 31 nm and was thermally stable up to 205°C. The surface area of MONT was measured to be 765 m²/g.

One of the representative electron-rich and redox-active organic systems is triphenylamine. The triphenylamine is known to show reversible one-electron oxidation reaction to generate a cationic radical species (Figure 7). Recently, there have been many papers on the synthesis of POP materials using triphenylamine derivatives as building blocks.²⁰

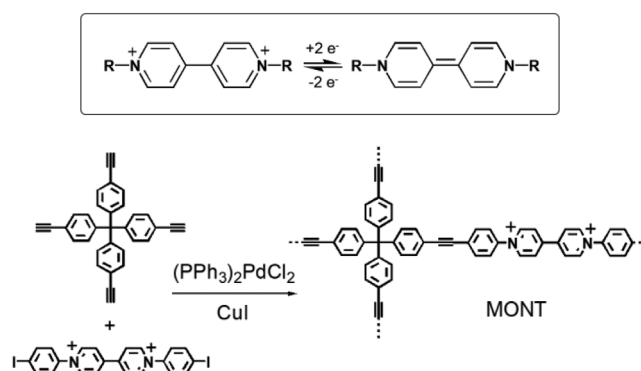


Figure 6. Two-electron redox conversion of viologen derivatives and the synthesis of POP bearing viologens through the Sonogashira coupling of tetra(4-ethynylphenyl)methane with di(4-iodophenyl)viologen salt. Reproduced under permission of ref. 19. Copyright 2012, Wiley-VCH.

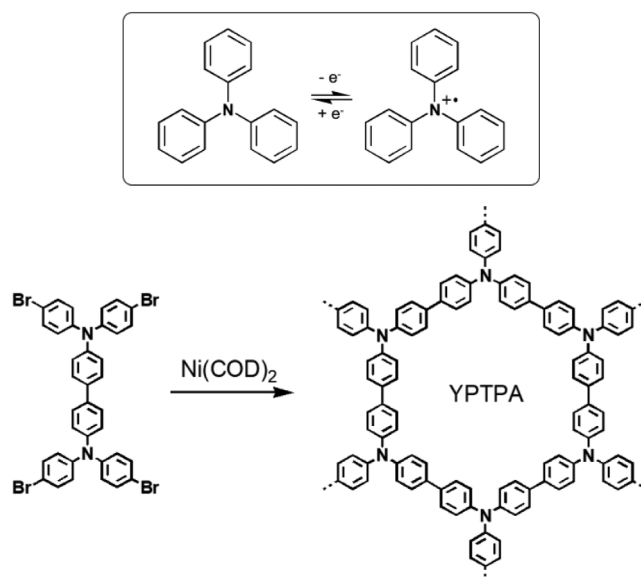


Figure 7. One-electron redox conversion of triphenylamine and the synthesis of POP-bearing triphenylamines by the Ni(COD)₂-catalyzed Yamamoto coupling of tetrakis(4-bromophenyl)biphenyl-4,4'-diamine. Reproduced under permission of ref. 22. Copyright 2016, Elsevier.

Those POP materials have been applied to various purposes including gas adsorbents.²¹

In 2016, Jiang and coworkers reported the preparation of redox-active POP-bearing triphenylamine moieties.²² The POP was prepared by the Yamamoto coupling of tetrakis(4-bromophenyl)biphenyl-4,4'-diamine. The resultant POP was denoted by YPTPA, showing a high surface area up to 1557 m²/g and microporosity.

Carbazoles with aromatic substituents are redox-active cyclic compounds bearing triphenylamines. The carbazoles are also known to show reversible one-electron oxidation reaction (Figure 8).

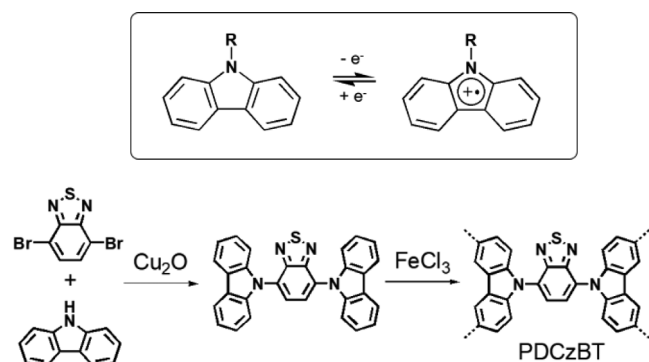


Figure 8. One-electron oxidation conversion of a carbazole derivative and the synthesis of POP-bearing carbazole moieties by the Friedel–Craft reaction of dicarbazolylbenzothiadiazole building block. Reproduced under permission of ref. 23. Copyright 2015, Royal Society of Chemistry.

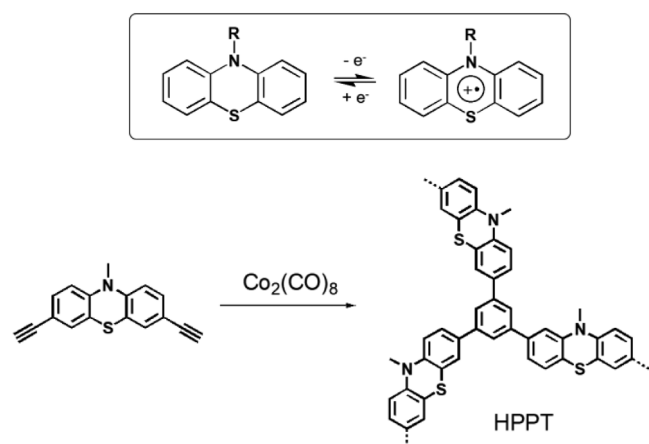


Figure 9. One-electron oxidation of phenothiazine derivatives and the synthesis of POP-bearing phenothiazines by the $\text{Co}_2(\text{CO})_8$ -catalyzed $[2 + 2 + 2]$ cyclization of *N*-methyl-3,7-diethynylphenothiazine. Reproduced under permission of ref. 24. Copyright 2020, Royal Society of Chemistry.

Carbazole derivatives have been utilized as building blocks in the synthesis of POP materials.²³ In 2015, Huang and coworkers reported the synthesis of conjugated microporous polymers bearing carbazoles (denoted by PDCzBT). The dicarbazolylbenzothiadiazole building block was prepared by the Cu_2O -catalyzed coupling of carbazole with benzothiadiazole. Through the analysis of N_2 adsorption–desorption isotherm curves, the surface area and pore volume of PDCzBT were measured to be $1166 \text{ m}^2/\text{g}$ and $0.7 \text{ cm}^3/\text{g}$, respectively. The PDCzBT was thermally stable up to 350°C .

Phenothiazines are known to show a reversible one-electron oxidation reaction (Figure 9).

While the phenothiazines have been utilized as redox-active species in the electrochromic devices, the POP materials with phenothiazines are relatively less explored.²⁴ In

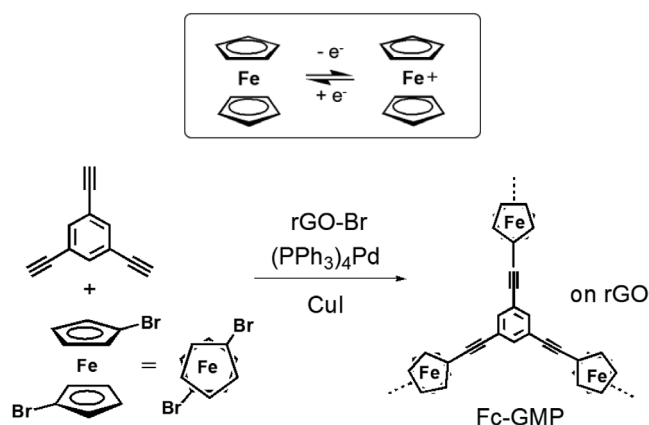


Figure 10. One-electron oxidation of ferrocene and the synthesis of POP-bearing ferrocenes on the reduced graphene oxide (rGO) by the Sonogashira coupling of 1,3,5-triethynylbenzene with 1,1'-dibromoferrocene in the presence of 4-bromophenyl terminated rGO. Reproduced under permission of ref. 25. Copyright 2018, Royal Chemical Society.

2020, Yang and coworkers reported the preparation of POP bearing phenothiazine moieties (denoted by HPPT) by the $\text{Co}_2(\text{CO})_8$ -catalyzed $[2 + 2 + 2]$ cyclization of *N*-methyl-3,7-diethynylphenothiazine.²⁴ The HPPT showed a high surface area of $452 \text{ m}^2/\text{g}$ and high thermal stability up to 421°C .

Ferrocene is a famous redox-active organometallic compound, showing chemical stability and reversible one-electron oxidation (Figure 10). Due to the electrochemical stability, the ferrocene has been utilized as a standard redox system of cyclic voltammetric studies of nonaqueous systems. Recently, there have been synthetic efforts for the POP-bearing ferrocenes.²⁵

For example, 1,1'-dibromoferrocene has been used as a building block in the synthesis of redox-active POP.²⁵ In 2018, Tang *et al.* reported the synthesis of reduced graphene oxide (rGO) composite of POP bearing ferrocene (Fc-GMP) by the Sonogashira coupling of 1,3,5-triethynylbenzene with 1,1'-dibromoferrocene in the presence of 4-bromophenyl-terminated rGO. The content of rGO in the Fc-GMP was measured to be 5.3%. The Fc-GMP showed a high surface area of $800 \text{ m}^2/\text{g}$. According to the AFM studies, the thickness of Fc-GMP was measured to be $\sim 15 \text{ nm}$.

Energy Storage Performance of Redox-Active POPs for Batteries

The redox-active POP materials can be applied for electrical energy storage. If the redox conversions of the POP materials are reversible, the thermodynamically non-spontaneous redox reactions can be applied for the energy charging process. In another hand, the thermodynamically spontaneous redox reactions can be applied for the energy discharging process.¹ In this regard, the redox-active POP

materials have been applied as electrode materials for secondary batteries.^{13,14,17,18,22–24}

As displayed in Figure 11, the redox-active POP materials have been fabricated on the surface of current collector using the binder and conductive carbon slurry. Usually, the redox-active POP materials have been studied as cathode materials in the Li-half cells. The conventional anode material was lithium metal.

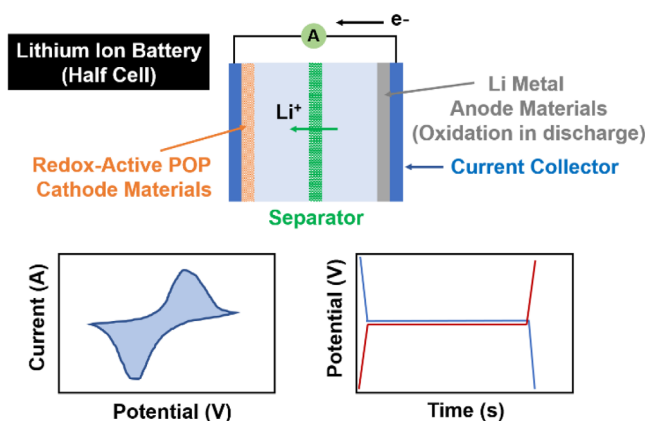


Figure 11. The structure of lithium ion battery (Li-half cell) which has been conventionally used for the redox-active POP materials and conventional patterns of cyclovoltammograms and charge-discharge profiles.

In the cyclic voltammetry, the redox-active POP materials showed conventional reduction and oxidation peaks. In the charging and discharging profiles, if the redox-active POP materials show clear plateaus, those materials can induce clear cell potentials in battery applications.

The recent electrochemical performance of the redox-active POP materials as cathode materials in the Li and Na-half cells was summarized in Table 1. At first, in the lithium ion batteries, the Poly-P5Q showed the capacities of 50.6 and 36.3 mAh/g at the current densities of 0.1 and 0.2 A/g, respectively¹³ (entries 1 and 2 in Table 1). The reduction potential of carbonyl groups of benzophenone moieties was observed at 2.23 V (vs Li/Li⁺). The charge transfer resistance (R_{CT}) was measured to be 77.3 Ω .

The IEP-11-E12 with anthraquinone moieties showed capacities of 69 and 47 mAh/g at the 5C and 30C conditions, as cathode materials for lithium ion batteries, respectively¹⁴ (entries 3 and 4 in Table 1). The charge/discharge potentials were located around 2.35 and 2.15 V (vs Li/Li⁺), respectively. Especially, the high surface area of IEP-11-E12 induced the enhanced electrochemical performance.

The PT-BTA-bearing pyrene-4,5,9,10-tetraone moieties showed the discharge capacities of 74.3, 58.6, and 35.0 mAh/g for lithium ion batteries at the current densities of 0.1, 0.2, and 1 A/g, respectively¹⁷ (entries 5 and 7 in Table 1). The PT-BTA showed two pairs of redox peaks at 2.05/2.70 and 2.65/2.36 V, respectively, indicating multiple redox processes. According to electrochemical impedance

Table 1. Electrochemical performance of redox-active POP as cathode electrode materials for batteries.

Entry	Materials	Capacities ^a (mAh/g)	Current Density (A/g)	Ref.
1	Poly-P5Q	50.6 (LIB)	0.1	13
2	Poly-P5Q	36.3 (LIB)	0.2	13
3	IEP-11-E12	69 (LIB)	5C	14
4	IEP-11-E12	47 (LIB)	30C	14
5	PT-BTA	74.3 (LIB)	0.1	17
6	PT-BTA	58.6 (LIB)	0.2	17
7	PT-BTA	35.0 (LIB)	1	17
8	H-MTPN-TCNE	120 (LIB)	0.1	18
9	H-MTPN-TCNE	107 (LIB)	0.2	18
10	H-MTPN-TCNE	80 (LIB)	1	18
11	H-MTPN-TCNE	72 (LIB)	2	18
12	YPTPA	97.6 (LIB)	2	22
13	PDCzBT	1042 (LIB)	0.02	23
14	PDCzBT	404 (LIB)	0.1	23
15	PDCzBT	312 (LIB)	0.2	23
16	PDCzBT	145 (SIB)	0.02	23
17	PDCzBT	119 (SIB)	0.05	23
18	PDCzBT	99 (SIB)	0.1	23
19	HPPT	93 (LIB)	0.2	24
20	HPPT	87 (LIB)	0.4	24
21	HPPT	75 (LIB)	0.8	24

^a LIB and SIB in parentheses imply lithium ion batteries and sodium ion batteries, respectively.

spectroscopy (EIS), the R_{CT} of PT-BTA in the coin-cell batteries was measured to be 72 Ω .

The H-MTPN-TCNE bearing 1,1,4,4-tetracyanobutadiene moieties showed discharge capacities of 120, 107, 80, and 72 mAh/g for lithium ion batteries at the current densities of 0.1, 0.2, 1, and 2 A/g, respectively¹⁸ (entries 8–11 in Table 1). While the main redox potential of discharging process was observed at ~ 3.75 V (vs Li/Li⁺), additional redox reactions were observed in the potential range of 1.5–3.0 V. While the H-MTPN without post-synthetic modification showed the R_{CT} of 165 Ω , the R_{CT} of H-MTPN-TCNE was measured to be 93 Ω , indicating that the introduction of 1,1,4,4-tetracyanobutadiene moieties to H-MTPN induced the compatible contact of cathode materials with electrolyte solution.

The YPTPA containing triphenylamines showed a discharge capacity of 97.6 mAh/g at the current density of 2 A/g for lithium ion battery²² (entry 12 in Table 1). The oxidation and reduction peaks of YPTPA were observed at 3.71 and 3.74 V (vs Li/Li⁺), respectively. The R_{CT} of YPTPA was measured to be 319 Ω .

The PDCzBT-bearing carbazoles and benzothiadiazoles showed the capacities of 1042, 404, and 312 mAh/g at the current densities of 0.02, 0.1, and 0.2 A/g, respectively, for lithium ion batteries²³ (entries 13–15 in Table 1). In addition, the PDCzBT was applied as a cathode material for sodium ion batteries and it showed 145, 119, and 99 mAh/g at the current densities of 0.02, 0.1, and 0.2 A/g, respectively (entries 16–18 in Table 1). Interestingly, major redox contribution of the PDCzBT was observed in the potential range of 0–0.5 V (vs Li/Li⁺ and vs Na/Na⁺).

The HPPT containing phenothiazine moieties showed discharge capacities of 93, 87, and 75 mAh/g at the current densities of 0.2, 0.4, and 0.8 A/g, respectively, for lithium ion batteries²⁴ (entries 19–21 in Table 1). It showed cathodic and anodic peaks at 3.78 and 3.47 V (vs Li/Li⁺), respectively.

Energy Storage Performance of Redox-Active POPs for Pseudocapacitors

Recently, supercapacitors also have been considered as promising energy storage devices,²⁶ in addition to batteries. While the supercapacitors that are based on capacitive energy storage have a merit of excellent power efficiency, due to the fast charge/discharge process, they have a critical disadvantage in energy storage capacity. In comparison, while the batteries that are based on redox energy storage have a merit of relatively high energy storage capacity, they have poor power efficiency, due to the relatively slow charge/discharge process.

Pseudocapacitors are advanced energy storage devices that are based on the combined capacitive and redox energy storage.^{1c} Thus, the electrode materials of pseudocapacitors should have both capacitive and redox behaviors. The comparison of device structures, cyclic voltammograms, and

charge–discharge profiles of the conventional capacitor and pseudocapacitor was displayed in Figure 12(a) and (b).

The POP with conjugated skeletons can be applied as electrode materials of supercapacitors. In addition, the redox-active POP materials with conjugated network structures can be applied as energy storage electrode materials for pseudocapacitor. Among the redox-active POP materials introduced in this review, the H-CMP-BPPB and Fc-GMP have been applied as electrode materials for pseudocapacitors.^{15,25} Their electrochemical performance was summarized in Table 2.

The H-CMP-BPPB bearing redox-active 1,4-di(3-phenylpropynoyl)benzene moieties showed capacitances of 220 and 120 F/g at the current densities of 0.5 and 10 A/g, respectively, in the symmetric coin cell supercapacitors.¹⁵ Interestingly, according to the EIS studies, the R_{CT} of H-CMP-BPPB in the current collector was measured to be 5.9 Ω , which is attributable to the hollow structure and thin shell thickness of 23 nm. Interestingly, the shell thickness of H-CMP-BPPB increased from 23 nm to 38 nm through the charge/discharge cycling.

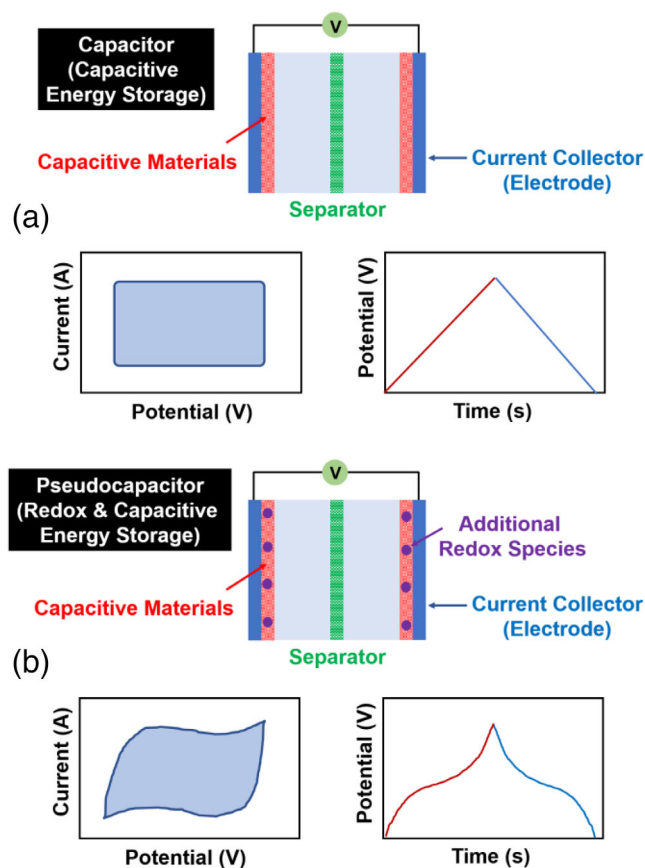


Figure 12. The structures of (a) capacitor (based on capacitive energy storage) and (b) pseudocapacitor (based on the combined capacitive and redox energy storage) devices and their conventional patterns of cyclic voltammograms and charge–discharge profiles.

Table 2. Electrochemical performance of redox-active POP as electrode materials for pseudocapacitors.

Entry	Materials	Capacitances ^a (F/g)	Current Density (A/g)	Ref.
1	H-CMP-BPPB	220 (two)	0.5	15
2	H-CMP-BPPB	120 (two)	10	15
3	Fc-GMP	470 (three)	0.5	25
4	Fc-GMP	231 (two)	0.5	25
5	Fc-GMP	246 (three)	10	25

^aTwo and three imply two-electrode devices and three-electrode cyclic voltammetric measurements, respectively.

The Fc-GMP-bearing ferrocene moieties showed capacitances of 470 and 246 F/g at the current densities of 0.5 and 10 A/g, respectively, in the three-electrode cyclic voltammetric test system.²⁵ The Fc-GMP maintained the capacitance of 231 F/g at the current density of 0.5 A/g in the two-electrode device. The high capacitances are attributable to the rGO contents in the materials. The R_{CT} of Fc-GMP-based electrode was measured to be 8.48 Ω , indicating the enhanced conductivity by the rGO in the materials.

Conclusion and Perspective

Through investigation of the recent redox-active POP materials, it became clear that the POP has a striking synthetic merit of facile chemical engineering. Various redox-active moieties could be incorporated into POP through the pre-designed building block approach and postsynthetic modification strategy. Due to the high surface area, porosity, and chemical stability, the redox-active POP materials could be successfully applied as electrode materials for batteries and pseudocapacitors. The redox-active POP materials have been mainly applied as cathode materials for batteries. Due to the insoluble feature of POP materials, the batteries and pseudocapacitors fabricated with leaching-free POP showed good cycling performance.

However, the critical weak points of the redox-active POPs as energy storage materials are their poor conductivities and the limitation of energy storage capacities. These problems can be overcome through the chemical engineering of functional composites. The advanced composite materials with the redox-active POP and functional inorganic materials (such as conducting or redox-active inorganic materials) can be developed. In addition, the morphology engineering of the redox-active POP materials can enhance the electrochemical performance, due to the reduced diffusion pathways of electrolyte solution into the electrode materials. Thus, the morphology-engineered POP-inorganic composites can be future research direction of development of advanced redox-active POP materials.

Acknowledgments. This work was supported by the National Research Foundation of Korea (NRF) grant (No. 2020R1A2C200431011) funded by the Korea government (MSIT) and the grant CAP-15-02-KBSI (R&D

Convergence Program) of National Research Council of Science & Technology (NST) of Korea.

Conflict of interest

The authors declare no conflict of interest.

References

- a) M. S. Whittingham, *Chem. Rev.* **2004**, *104*, 4271. b) M. Winter, B. Barnett, K. Xu, *Chem. Rev.* **2018**, *118*, 11433. c) Y. Jiang, J. Liu, *Energy Environ. Mater.* **2019**, *2*, 30.
- H. Wang, C. -J. Yao, H. -J. Nie, K. -Z. Wang, Y. -W. Zhong, P. Chen, S. Mei, Q. Zhang, *J. Mater. Chem. A* **2020**, *8*, 11906.
- L. Croguennec, M. R. Palacin, *J. Am. Chem. Soc.* **2015**, *137*, 3140.
- a) C. Han, H. Li, R. Shi, T. Zhang, J. Tong, J. Li, B. Li, *J. Mater. Chem. A* **2019**, *7*, 23378. b) K. Amin, L. Mao, Z. Wei, *Macromol. Rapid Commun.* **2019**, *40*, 1800565.
- M. Armand, J.-M. Tarascon, *Nature* **2008**, *451*, 652.
- a) Y. Liang, Y. Yao, *Joule* **2018**, *2*, 1690. b) J. Heiska, M. Nisula, M. Karppinen, *J. Mater. Chem. A* **2019**, *7*, 18735.
- a) J.-S. M. Lee, A. I. Cooper, *Chem. Rev.* **2020**, *120*, 2171. b) B. Zheng, X. Lin, X. Zhang, D. Wu, K. Matyjaszewski, *Adv. Funct. Mater.* **2019**, *30*, 1907006. c) N. Chaoui, M. Trunk, R. Dawson, J. Schmidt, A. Thomas, *Chem. Soc. Rev.* **2017**, *46*, 3302. d) L. Tan, B. Tan, *Chem. Soc. Rev.* **2017**, *46*, 3322. e) S. Das, P. Heasman, T. Ben, S. Qiu, *Chem. Rev.* **2017**, *117*, 1515. f) J.-K. Sun, M. Antonietti, J. Yuan, *Chem. Soc. Rev.* **2016**, *45*, 6627. g) Y. Xu, S. Jin, H. Xu, A. Nagai, D. Jiang, *Chem. Soc. Rev.* **2013**, *42*, 8012. h) F. Vilela, K. Zhang, M. Antonietti, *Energy Environ. Sci.* **2012**, *5*, 7819. i) D. Wu, F. Xu, B. Sun, R. Fu, H. He, K. Matyjaszewski, *Chem. Rev.* **2012**, *112*, 3959.
- K. Cho, S. M. Lee, H. J. Kim, Y.-J. Ko, E. J. Kang, S. U. Son, *Chem. Eur. J.* **2020**, *26*, 788.
- S. K. Chae, K. Cho, S. M. Lee, H. J. Kim, Y. J. Ko, S. U. Son, *Polym. Chem.* **2020**, *11*, 789.
- C. W. Kang, J. H. Ko, S. M. Lee, H. J. Kim, Y.-J. Ko, S. U. Son, *J. Mater. Chem. A* **2019**, *7*, 7859.
- N. Kang, J. H. Park, M. Jin, N. Park, S. M. Lee, H. J. Kim, J. M. Kim, S. U. Son, *J. Am. Chem. Soc.* **2013**, *135*, 19115.
- a) D. H. Lee, K. C. Ko, J. H. Ko, S. Y. Kang, S. M. Lee, H. J. Kim, Y. -J. Ko, J. Y. Lee, S. U. Son, *ACS Macro Lett.* **2018**, *7*, 651. b) S. Y. Kang, C. W. Kang, D. W. Kim, Y. Myung, J. Choi, S. M. Lee, H. J. Kim, Y. -J. Ko, S. U. Son, *Chem. Asian J.* **2019**, *14*, 3173.

13. A. Ahmad, Q. Meng, S. Melhi, L. Mao, M. Zhang, B. -H. Han, K. Lu, Z. Wei, *Electrochim. Acta* **2017**, 255, 145.
 14. A. Molina, N. Patil, E. Ventosa, M. Liras, J. Palma, R. Marcilla, *Adv. Func. Mater.* **2020**, 30, 190874.
 15. J. Choi, J. H. Ko, C. W. Kang, S. M. Lee, H. J. Kim, Y. -J. Ko, M. Yang, S. U. Son, *J. Mater. Chem. A* **2018**, 6, 6233.
 16. S. Y. Park, C. W. Kang, S. M. Lee, H. J. Kim, Y. -J. Ko, J. Choi, S. U. Son, *Chem. Eur. J.* **2020**, 26, 12343.
 17. K. Li, Q. Li, Y. Wang, H.-G. Wang, Y. Li, Z. Si, *Mater. Chem. Front.* **2020**, 4, 2697.
 18. J. Choi, E. S. Kim, J. H. Ko, S. M. Lee, H. J. Kim, Y. -J. Ko, S. U. Son, *Chem. Commun.* **2017**, 53, 8778.
 19. N. Kang, J. H. Park, J. Choi, J. Jin, J. Chun, I. G. Jung, J. Jeong, J. -G. Park, S. M. Lee, H. J. Kim, S. U. Son, *Angew. Chem. Int. Ed.* **2012**, 51, 6626.
 20. J. H. Ko, N. Kang, N. Park, H. -W. Shin, S. Kang, S. M. Lee, H. J. Kim, T. K. Ahn, S. U. Son, *ACS Macro Lett.* **2015**, 4, 669.
 21. X. Yang, S. Yao, M. Yu, J. -X. Jiang, *Macromol. Rapid Commun.* **2014**, 35, 834.
 22. C. Zhang, X. Yang, W. Ren, Y. Wang, F. Su, J. -X. Jiang, *J. Power Sources* **2016**, 317, 49.
 23. S. Zhang, W. Huang, P. Hu, C. Huang, C. Shang, C. Zhang, R. Yang, G. Cui, *J. Mater. Chem. A* **2015**, 3, 1896.
 24. Y. Zhang, P. Gao, X. Guo, H. Chen, R. Zhang, Y. Du, B. Wang, H. Yang, *RSC Adv.* **2020**, 10, 16732.
 25. A. M. Khattak, H. Sin, Z. A. Ghazi, X. He, B. Liang, N. A. Khan, H. R. Alanagh, A. Iqbal, L. Li, Z. Tang, *J. Mater. Chem. A* **2018**, 6, 18827.
 26. S. Najib, E. Erdem, *Nanoscale Adv.* **2019**, 1, 2817.
-